Proceedings of the IASS 2024 Symposium
Redefining the Art of Structural Design
August 26-30, 2024, Zurich Switzerland
Philippe Block, Giulia Boller, Catherine DeWolf,
Jacqueline Pauli, Walter Kaufmann (eds.)

Formulation of elastic stress in the fiber transverse direction of full-culm bamboo subjected to bending

Takuo NAGAI*

*Department of Design and Architecture, University of Shiga Prefecture
2500, Hassaka-cho, Hikone-city, Shiga, Japan
nagai.t@ses.usp.ac.jp / nagaitakuo@gmail.com

Abstract

Bamboo not only excels in regenerative power and possesses high strength but also features a lightweight and hollow cross-section in its natural form, making it highly useful as a structural material for spatial structures. This paper aims to promote the future use of bamboo in spatial structures and discusses the bending failure mechanism of bamboo culms. When bamboo culms undergo bending along the culm axis, the orthogonal cross-section flattens, leading to maximum load due to bending failure in the direction perpendicular to the fibers in the culm wall. Therefore, evaluating the bending stress in the perpendicular direction of fibers, which occurs in conjunction with bending along the culm axis, becomes crucial in estimating the bending strength of bamboo culms. This study formulates the stresses occurring in the culm wall under bending based on the Brazier effect theory and compares the results with bending experiments conducted on Madake and Moso bamboo. The experiments confirmed that the strains in the fiber perpendicular direction within the culm wall align well with the Brazier effect theory in the micro-deformation region. Furthermore, the strain in the fiber perpendicular direction of the culm wall at the point of bending failure corresponded well with that determined by the small-scale edge bearing test.

Keywords: Full-culm bamboo, Bending failure, Brazier effect theory, Anisotropy, Edge bearing test

1. Introduction

Bamboo is considered to possess a high potential as a material for architectural structures, especially as structural material for spatial structures, due to its rapid growth and regenerative abilities, high strength and stiffness, and its characteristics of being hollow and lightweight. In recent years, substantial bamboo spatial structures have been realized in South Asia and South America (e.g., The Arc at Green School Bali [1], Vo Trong [2]). The methods of utilizing bamboo culms in these structures can be broadly classified into three categories: (i) cutting the bamboo culms into relatively short lengths for use as trusses or lattices (see works by Renzo Piano Building Workshop or Shoei Yoh, e.g. [3], [4]), (ii) applying a “Rup-Rup” technique to the bamboo culms before bending them for use as arches [1], and (iii) introducing elastic bending to unprocessed bamboo culms for use as bending-active elements (e.g. [2], [5]). In particular, the last method is an effective technique for achieving high stiffness with a minimal amount of resources, and can be said to make good use of the high strength and flexibility of bamboo culms.

However, at present, the bamboo species for which material properties are defined in design codes of various countries are very limited, and extensive experimentation is required for the design of bamboo structures using other bamboo species, which necessitates a significant amount of time and effort. Specifically, because understanding the bending characteristics of bamboo culms requires elaborate loading equipment and a large number of samples, to establish simpler testing methods is desired. Therefore, this study theoretically examines the bending failure mechanisms and determinants of

bending strength of bamboo culms and explores a method for simply estimating bending strength without conducting bending tests on lengthy specimens.

2. Formulation of stress distribution in bamboo culms subject to bending

2.1. Brazier effect theory

As shown in Fig. 1(a) and (b), when a bamboo culm undergoes pure bending along the culm axis (*x*-axis), the orthogonal cross-section deforms into an elliptical shape due to the Brazier effect ([6]~[7]), resulting in bending along the circumferential direction of the culm wall. This deformation of the cross-section can lead to local buckling or circumferential bending failure in the culm wall, ultimately causing the bamboo culm to fail under bending. Therefore, to estimate the bending strength of bamboo culms, it is necessary to quantitatively evaluate the deformation of the cross-section caused by the Brazier effect. This paper presents an overview of the formulation of the Brazier effect, following previous studies ([6]~[9]). In the cross-section of a bamboo culm, the four intersection points along the *y* - *z* axis and the *s* axis are designated as points N, S, E, and W (Fig. 1(c)). Furthermore, the reduction ratio of the cross-sectional height at points N and S after deformation is expressed as the flattening ratio ζ. E_x represents the bending Young's modulus in the direction parallel to the fibers, while E_s represents that in the perpendicular direction to the fibers.

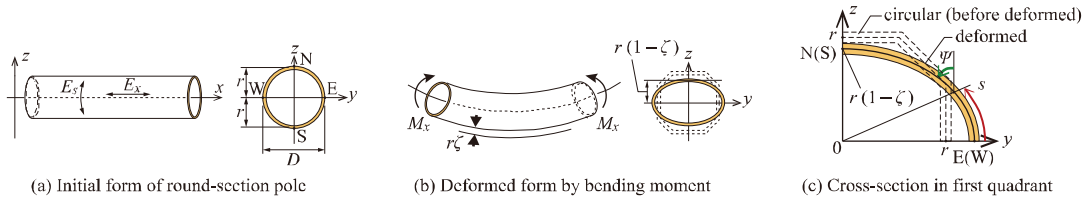

(a) Initial form of round-section pole (b) Deformed form by bending moment (c) Cross-section in first quadrant

Figure 1: The brazier effect on the cross-section of a cylindrical member and the definition of coordinates and variables.

The curvature of the culm wall along the s-axis after deformation is expressed using the tangent angle ψ as follows ([7], [9]).

$$\frac{d\psi}{ds} = \frac{1}{r} + \frac{3\Gamma}{r}\cos\frac{2s}{r}, \qquad r = \frac{D-t}{2} \tag{1}$$

The second term on the right side of the above equation represents the deformation due to the Brazier effect, where Γ is a constant unrelated to the coordinate *s*. The total potential energy is derived for a free body extracted per unit length in the *x*-axis direction as shown in Fig. 1(b), subjected to bending moments M_x at both ends. First, the strain energy in the *x*-axis direction is expressed as follows.

$$U_x = \frac{E_x I \cdot f(\Gamma)}{2}\kappa^2, \qquad f(\Gamma) = 1 - \frac{3}{2}\Gamma - \frac{1}{2}\Gamma^2 + \frac{21}{16}\Gamma^3 + \cdots \tag{2}$$

Here, κ represents the curvature along the *x*-axis, *I* is the second moment of area before deformation, and $f(\Gamma)$ denotes the reduction ratio of the second moment of area due to deformation of the section. Next, the total bending strain energy in the direction perpendicular to the fibers is obtained by integrating the square of the second term on the right side of Eq. (1) over one complete revolution along the *s*-axis, as follows.

$$U_s = \oint \frac{1}{2}\cdot\frac{E_s t^3}{12}\left(\frac{3\Gamma}{r}\cos\frac{2s}{r}\right)^2 ds = \frac{3}{2}\frac{\pi E_s t^3}{r}\Gamma^2 \tag{3}$$

Consequently, the total potential energy in this free body can be expressed as follows.

$$\Pi = U_x + U_s - M_x\kappa \tag{4}$$

By setting the partial derivatives with respect to the deformation parameters κ and Γ to zero in the above equation, the following equilibrium equations can be obtained.

$$M_x = E_x I \cdot f(\Gamma)\kappa \tag{5}$$

$$\frac{63}{32}E_x I\kappa^2\Gamma^2 + \left(\frac{3}{2}\frac{\pi E_s t^3}{D} - \frac{E_x I}{2}\kappa^2\right)\Gamma - \frac{3}{4}E_x I\kappa^2 = 0 \tag{6}$$

In addition, the bending moment per unit width in the *s*-axis direction (perpendicular to the fibers) occurring in the culm wall is expressed by the following equation.

$$M_s = \frac{E_s t^3}{12}\cdot\left(\frac{d\psi}{ds} - \frac{1}{r}\right) = \frac{E_s t^3}{12}\cdot\frac{3\Gamma}{r}\cos\frac{2s}{r} \tag{7}$$

2.2. Elastic constitutive equations within the culm wall

The stresses that occur in the culm wall when the bamboo culm is subjected to bending consist of the bending stress σ_{bx} in the fiber parallel direction, the bending stress σ_{bs} in the perpendicular direction due to the Brazier effect, and circumferential stress resulting from other factors (for example, prestress occurring during growth). However, since there is no direct method to determine the last component of stress, and it is considered to be smaller than the bending stresses in both directions on the inner and outer surfaces of the culm wall, this stress component will be ignored in the discussion here. Additionally, given that the t/D ratio (wall thickness to diameter ratio) for both Madake and Moso bamboo is approximately 0.06 to 0.09 at most parts of the culm [10], and considering that there are no external forces acting out of plane in this discussion, it is assumed that the culm wall is in a state of plane stress. Furthermore, since the fibers of the bamboo are aligned parallel to the culm axis, anisotropy in the plane is assumed for the culm wall, and the elastic constitutive equations are expressed as follows.

$$\varepsilon_x = \frac{1}{E_x}\sigma_{bx} - \frac{\nu_{sx}}{E_s}\sigma_{bs} \tag{8}$$

$$\varepsilon_s = -\frac{\nu_{xs}}{E_x}\sigma_{bx} + \frac{1}{E_s}\sigma_{bs} \tag{9}$$

Here, ε_x and ε_s represent strain in each direction, while ν_{xs} and ν_{sx} are the Poisson's ratios corresponding to these strains. In the formulation of this paper, pure bending is assumed, and shear deformation is ignored. Furthermore, due to the symmetry of the constitutive equations, since $E_x\nu_{sx} = E_s\nu_{xs}$, it follows that only three elastic constants, for instance, E_x, E_s, and ν_{xs}, need to be determined experimentally. Henceforth, the stresses and strains in the direction perpendicular to the fibers determined based on the above formulation will be referred to as the Brazier effect theoretical values (BET).

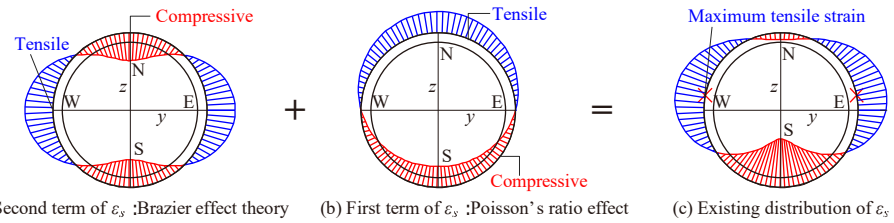

(a) Second term of ε_s :Brazier effect theory (b) First term of ε_s :Poisson's ratio effect (c) Existing distribution of ε_s

Figure 2: Diagram of strain distribution on the outer surface in the direction perpendicular to the fibers.

Fig. 2 is a conceptual diagram showing the distribution of strain ε_s in the direction perpendicular to the fibers on the outer skin of a bamboo culm when it is subjected to bending with compression at the upper end. (a) represents the second term of Eq. (9) (strain due to the Brazier effect), assuming mirror-symmetrical deformation with respect to the *y*-*z* axis, resulting in the maximum strain occurring at points N, S, E, and W. Additionally, (b) corresponds to the first term of Eq. (9). The distribution of strain is represented as the sum of these, as shown in (c), indicating that the maximum tensile strain occurs slightly above points E and W.

3. Bending and other preliminary test methods

3.1. Materials and test procedures

This study conducts experiments on Madake bamboo (*Phyllostachys bambusoides*) and Moso bamboo (*Phyllostachys edulis*). Both were collected from a bamboo forest in Omihachiman-city, Shiga Prefecture (35°15'N, 136°09'E), and were stored outdoors for several weeks to half a year after cutting, protected from rain and wind. Additionally, due to the short storage period, no protective treatments were applied.

As mentioned in the previous chapter, to evaluate the behavior of bamboo culms in the direction perpendicular to the fibers under bending, it is necessary to identify multiple values of elastic constants. Firstly, as a preliminary experiment, the Poisson's ratio of the bamboo culm wall is determined through a short column compression test, and the bending characteristics in the direction perpendicular to the fibers are verified through a edge bearing test. Subsequently, the strain at multiple points of the bamboo culm during the bending test is measured to verify consistency with the BET values.

3.2. Measurement of Poisson's ratio

The measurement of Poisson's ratio is conducted using the test method "10. Compression strength and stiffness parallel to the fibres" from ISO 22157 [11], hereafter referred to as the "short column compression test." The test method is illustrated in Fig. 3. Strain gauges are affixed at two opposing points on the outer and inner skins at the mid-height of the specimen, in both the direction parallel and perpendicular to the fibers, measuring strain at a total of eight points. Here, it is assumed that the stress in the direction perpendicular to the fibers is zero, and the Young's modulus and Poisson's ratio in the direction parallel to the fibers are determined using the following formula.

$$E_x = \frac{\sigma_{x,60} - \sigma_{x,20}}{\varepsilon_{x,60} - \varepsilon_{x,20}} \tag{10}$$

$$\nu_{xs} = -\frac{\varepsilon_{s,60} - \varepsilon_{s,20}}{\varepsilon_{x,60} - \varepsilon_{x,20}} \tag{11}$$

Here, X_{20} and X_{60} refer to the measurements at 20% and 60% of the maximum load, respectively. The calculation of the Young's modulus is conducted as outlined in ISO 22157, and the calculation of the Poisson's ratio follows a similar procedure.

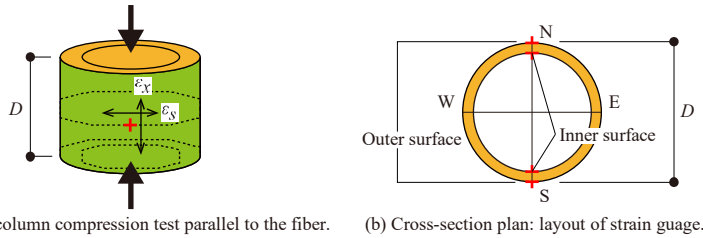

(a) Short-column compression test parallel to the fiber. (b) Cross-section plan: layout of strain guage.

Figure 3: Method of measuring strain for calculating Poisson's ratio in compression tests.

Table 1 presents the results for the Poisson's ratio of each specimen. $\nu_{xs,in}$ is the measurement for the inner skin, while $\nu_{xs,out}$ is for the outer skin. There are a total of six specimens, comprising three of Madake and three of Moso bamboo. Generally, the Young's modulus in the direction parallel to the fibers E_x, has a negative correlation with the culm diameter ([12], [13]), and thus, in this experiment, the specimens with larger diameters have the smallest values of E_x. The values of ν_{xs} show considerable variability, and no significant trends can be observed in comparisons either between bamboo species or between the inner and outer sides of the culm walls. The statistical analysis of Poisson's ratio remains a topic for future study; for now, an average value of 0.26, encompassing all eight values from both bamboo species and both the inner and outer skins, will be used for further discussion. It is worth noting,

for example, that Ario *et al*. [14] have measured the Poisson's ratio v_{xs} of the culm wall of Moso bamboo harvested in Japan, finding it to be around 0.3 for the outer skin. Similarly, pioneers in the study of physical properties of bamboo, such as Janssen [15], have determined the Poisson's ratio for Guadua bamboo from South America to be approximately 0.3, which is close to the results obtained in this study.

Table 1: Measured Poisson's ratio for each specimen.

Specimen	D [mm]	t [mm]	E_x [MPa]	$v_{xs,\text{in}}$	$v_{xs,\text{out}}$	MC [%]
Madake-1	59.4	3.8	20940	0.27	0.31	9.38
Madake-2	82.4	5.0	24140	0.28	0.17	11.94
Madake-3	111.0	6.5	6770	0.33	0.25	14.86
Moso-1	63.6	5.8	12750	0.14	0.10	11.44
Moso-2	77.5	5.5	18464	0.33	0.36	10.00
Moso-3	105.6	7.5	9102	0.30	0.28	27.70
Mean value				0.28	0.24	

Note: out = outer surface, in = inner surface, MC = moisture content ratio

3.3. Bending tests perpendicular to the fibers

The measurement of the bending characteristics of bamboo culm walls in the direction perpendicular to the fibers is conducted in accordance with "15. Bending strength and stiffness perpendicular to the fibres" of ISO 22157, hereinafter referred to as the "edge bearing test" ([16], [17]). Moreover, the edge bearing test in ISO 22157 can result in two modes of failure, either at the NS or EW points, but predicting which will occur is challenging. Therefore, edge bearing tests with pre-installed bending hinges on the bamboo culm specimens are also conducted (Nagai *et al*. [6]).

Fig. 4 shows the method of sampling test specimens from bamboo culms and the testing method. For each of Madake and Moso bamboo, three consecutive specimens are taken from a single bamboo culm, designated for NS-hinged, EW-hinged, and ISO (non-hinged) testing, respectively. To measure the maximum bending strain at the failure points in each failure mode, strain gauges are attached at four locations on the inner and outer skins at points E and W for the NS-hinged specimens, and at four locations on the inner and outer skins at points N and S for the EW-hinged specimens.

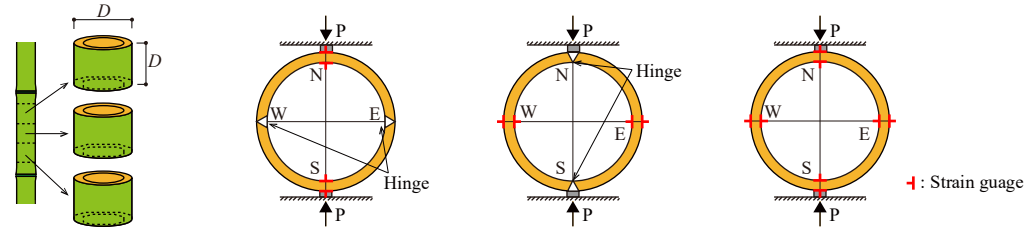

(a) Sampling method (b) EW-hinge test (c) NS-hinge test (d) Edge bearing test (ISO 22157)

Figure 4: Method for measuring strain to calculate properties perpendicular to the fibers in edge bearing tests.

Table 2: Measured strain at maximum load in each edge bearing test.

Species	Test method	D [mm]	t [mm]	MC [%]	Maximum strain at mesured loacation								
					N		S		E		W		
					out	in	out	in	out	in	out	in	Mean
Madake	EWH	93.1	5.9	16.3	-1.47	**2.28**	-1.24	**2.55**					**2.41**
	NSH	92.1	5.5	18.4					**0.78**	-0.86	**0.69**	-0.82	**0.71**
	ISO	92.3	5.3	17.6	-1.02	1.65	-0.95	1.79	**0.71**	-0.88	**0.65**	-0.91	
Moso	EWH	93.3	7.4	36.4	-1.40	**1.71**	-1.49	**1.59**					**1.65**
	NSH	93.0	6.9	26.0					**0.68**	-0.76	**0.78**	-0.82	**0.72**
	ISO	92.7	7.6	17.0	-1.15	1.19	-0.94	1.06	**0.68**	-0.91	**0.76**	-0.92	

Note: EWH = EW-hinge test, NSH = NS-hinge test.
Unit of strain = %, out = outer surface, in = inner surface. **Bold** = strain at failure location

Table 2 shows the specifications of the specimens and the strains measured at various locations at maximum load. Positive values indicate tensile strain, while negative values indicate compressive strain. The strain on the inner side of the same location is greater in all tests compared to the outer side.

Furthermore, bold values represent the strain at locations where tensile failure occurred, and for both types of bamboo, the strain is smaller in cases where failure occurs on the outer skin.

3.4. Bending test method

Fig. 5 shows the method for bending test of bamboo culms and the locations for measuring strain. BT1 to BT3 are for Madake, and BT4 to BT6 are for Moso bamboo. The loading method used is a three-point bending with concentrated load applied at the center of the span. While ISO 22157 recommends a four-point bending test method for bamboo culms, studies such as Horie [18] have compared three-point and four-point bending and shown that there is no significant difference in bending strength. This is considered to be because the failure of bamboo culms does not occur in the pure bending section but is often preceded by failure at the loading point, leading to maximum load, a result also confirmed by the authors in preliminary experiments. Therefore, due to the limitations of the maximum span and displacement stroke possible with the experimental setup available to the authors, a three-point bending was chosen.

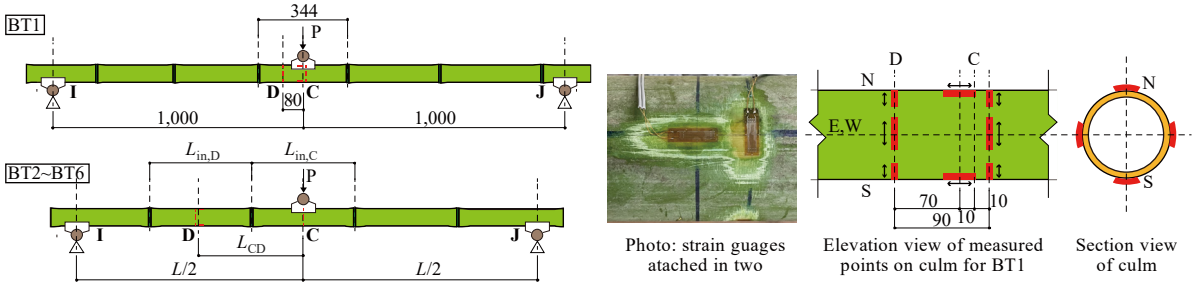

Figure 5: Left: method for bending test of bamboo culm. Right: strain measuring points in bending test specimens.

Table 3: Dimensions of specimens for the bending test.

Species			Madake			Moso		
Position	Dimension		BT1	BT2	BT3	BT4	BT5	BT6
C	D	[mm]	73.2	71.0	63.7	68.4	68.4	62.7
	t	[mm]	5.9	4.7	4.4	5.4	5.6	5.1
	$L_{in,C}$	[mm]	344	394	430	454	326	314
	$L_{in,C}/D$		4.7	5.5	6.8	6.6	4.8	5.0
D	D	[mm]	73.2	72.6	65.6	71.0	70.3	64.9
	t	[mm]	5.5	4.9	4.5	5.6	5.7	5.4
	$L_{in,D}$	[mm]	344	388	430	458	314	308
	$L_{in,D}/D$		4.7	5.3	6.6	6.5	4.5	4.7
I	D	[mm]	69.1	74.8	66.8	73.2	71.6	66.2
	t	[mm]	8.3	5.4	4.7	5.7	6.0	5.7
J	D	[mm]	73.2	67.5	60.5	64.6	65.2	59.8
	t	[mm]	5.3	4.7	4.4	6.0	5.4	5.0
L		[mm]	2000	1800	1800	1500	1500	1280
L_{CD}		[mm]	70	391	430	464	337	322

The loading point C is positioned exactly in the middle of the internode. Furthermore, following the ISO 22157 method, the loading span was determined to ensure a shear span ratio of more than 10. The strain measurement locations are all in the middle of an internode. For BT1, strain is measured in the fiber parallel direction at points N and S and in the fiber perpendicular direction at points N, S, E, and W at the loading point C, as well as at points N, S, E, and W in the fiber perpendicular direction at point D (a position avoiding the loading fixture) within the same internode as the loading point C. For BT2 to BT6, strain is measured in the fiber perpendicular direction at points N, S, E, and W at the loading point C, in the fiber parallel direction at points N and S, and in the fiber perpendicular direction at points N, S, E, and W in the middle of the internode adjacent to the internode containing the loading point (point D).

Although it is predicted that the fiber perpendicular direction bending failure of the culm wall occurs slightly above points E and W, as mentioned earlier, it is difficult to specify that location before the experiment, so the strain at points E and W, considered close to the potential failure location, is measured.

Table 3 shows the dimensional values for various parts of the test specimens. The bamboo poles used for the bending test specimens were all harvested from different bamboo culms. D and t represent the culm diameter and wall thickness at each measurement point, respectively, while L_{in} is the internode length at that measurement point. The ratio of internode length to diameter (L_{in}/D) at the locations where strain was measured ranges from 4.4 to 6.8. According to the method reported in Nagai *et al*. [6], when calculating the restraining effect of nodes due to the Brazier effect, it was found that at stress levels below 100 N/mm^2, the conditions do not produce a cross-sectional flattening restraint effect due to the nodes.

Additionally, after conducting the bending tests, specimens were extracted from the bamboo culms avoiding areas of high stress or damage, and were cross-sectioned for further mechanical tests including short column compression, hinged-edge bearing, and shear tests, as well as for measuring the moisture content and specific gravity of each specimen.

4. Results and discussion of bending tests

Table 4 presents the characteristic values of the specimens obtained from the tests. The photographs in Fig. 6 show examples near the central loading point at the time of bending failure. In all specimens, the maximum load was reached when splitting occurred slightly above points E and W along the culm axis, followed by a rapid decrease in load and subsequent splitting at points N and S, leading to the final state. The shear stress at the maximum load in all tests is assumed to be below 1.0 N/mm^2, which is considerably lower than the shear strength, indicating that this splitting is not due to shear failure.

Table 4: Measured mechanical and physical properties of specimens for the bending test.

Species		Madake				Moso			
Properties		BT1	BT2	BT3	Mean	BT4	BT5	BT6	Mean
MC	[%]	89.0	68.1	73.0	76.7	21.5	45.6	31.1	32.7
ρ_{dry}		0.64	0.69	0.69	0.67	0.60	0.82	0.82	0.75
f_c	[N/mm^2]	48.1	53.8	57.7	53.2	43.6	75.6	70.1	63.1
f_s	[N/mm^2]	9.1	11.9	13.6	11.5	10.0	14.1	15.1	13.1
f_{bx}	[N/mm^2]	80.3	95.5	95.3	90.4	98.7	108.2	101.3	102.7
E_{bx}	[N/mm^2]	17992.97	20713.88	20036.92	19581	14085.61	13355.71	16776.99	14739
$f_{bs,in}$	[N/mm^2]	23.0	25.4	28.2	25.5	26.8	43.7	48.9	39.8
$E_{bs,in}$	[N/mm^2]	1173	1238	1748	1386	1307	2634	2289	2077
$f_{bs,out}$	[N/mm^2]	10.8	11.5	11.1	11.1	11.8	15.3	18.8	15.3
$E_{bs,out}$	[N/mm^2]	1186	1319	1329	1278	2846	2846	2573	2755

Note: f_c = compression strength parallel to fibre, f_s = shear strength parallel to fibre,
f_{bx} = bending strength parallel to fibre, E_{bx} = bending Young's modulus parallel to fibre,
$f_{bs,in}$ = bending strength perpendicular to fibre, $E_{bs,in}$ = bending Young's modulus perpendicular to fibre,

Fig. 7(a) shows the relationship between the bending stress σ_{bx} (calculated) in the fiber parallel direction at the upper and lower edges (points N & S) of the loading point C for each specimen and the displacement at the loading point δ_c. σ_{bx} is calculated by dividing the bending moment at the loading point by the section modulus at the same location. Meanwhile, Fig. 7(b) illustrates the relationship between σ_{bx} and the fiber parallel direction strain ε_x (measured value), with the results at point C for BT1, and at point D for BT2 to BT6. σ_{bx} is calculated by dividing the bending moment at the measurement location by the section modulus for that location. The sign of the strain indicates tension as positive and compression as negative. The measurements for BT1, possibly due to being directly beneath the loading fixture, show a curve that significantly deviates from the others at points N (compression edge) and S (tension edge). In other tests, the strains at points N and S are almost symmetric and linear.

Figure 6: Photos of culm wall bending failure in the bending tests. Left: BT2; Right: BT5.

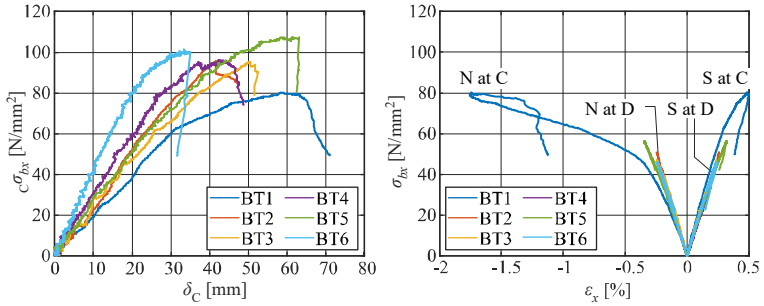

(a) Bending stress parallel to fiber vs vertical deformation at C

(b) Bending stress vs strain in direction parallel to fiber

Figure 7: Relationships between measured strain parallel to the fibers and calculated bending stress.

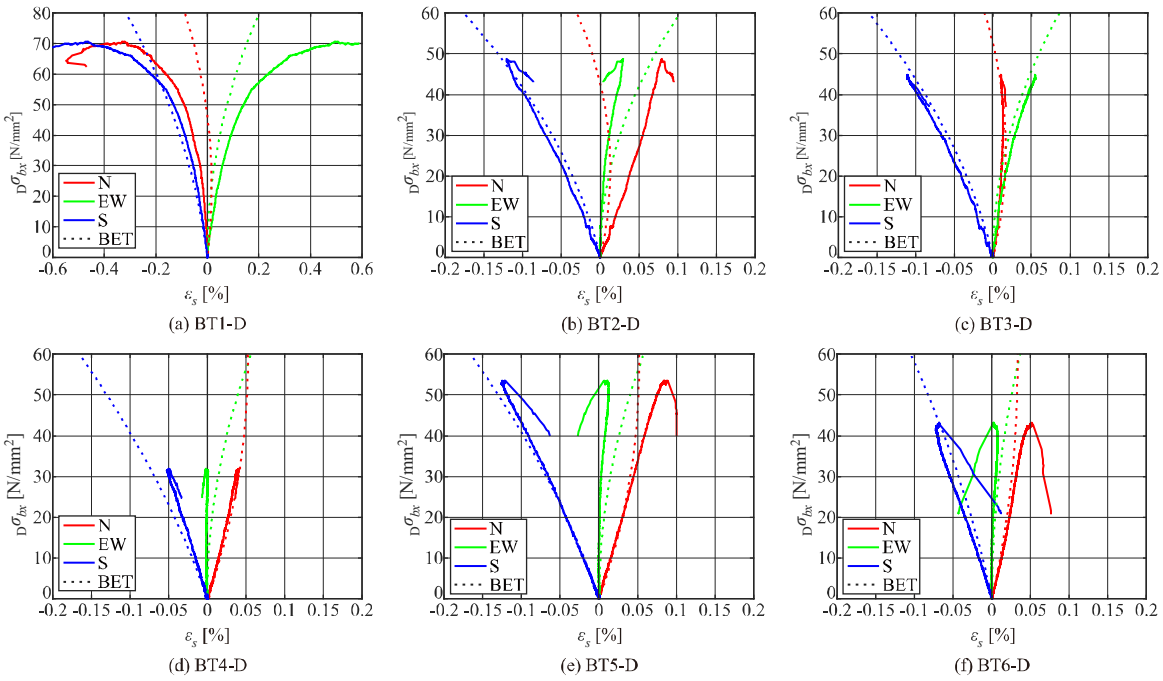

(a) BT1-D (b) BT2-D (c) BT3-D

(d) BT4-D (e) BT5-D (f) BT6-D

Figure 8: Relationships between measured strain perpendicular to the fibers and calculated bending stress.

Regarding the strain in the direction perpendicular to the fibers, only the results measured at point D are shown. This is because, at the loading point C, where the external force directly acts, the measured strain at each point significantly diverges from the BET values. Fig. 8 illustrates the relationship between the bending stress σ_{bx} (calculated value) in the fiber parallel direction and the fiber perpendicular direction strain ε_s (measured value) at point D. "EW" represents the average value of strains at points E and W. The dotted lines are the values based on BET for each measurement location, calculated using the cross-sectional dimensions at the measurement points and the Young's moduli in both parallel and

perpendicular directions to the fibers. For these calculations, the value of v_{xs} was taken as 0.26, the Young's modulus in the fiber parallel direction for each specimen was taken from E_{bx}, and the Young's modulus in the perpendicular direction was the average of $E_{bs,\text{in}}$ and $E_{bs,\text{out}}$ in Table 4. Except for BT1, where the central loading point C and point D are closely situated, the results generally align well with BET, with BT3 and BT4 showing good agreement across all load levels, and BT5 and BT6 aligning very closely at lower load levels. Therefore, despite some variability among specimens, it can be said that the formulation based on the Brazier effect theory is very effective in some cases.

Table 5 summarizes the average strain values at points E and W at the maximum load for each test. Compared to the maximum bending strain in the direction perpendicular to the fibers (about 0.7%) obtained from the edge bearing test mentioned in the previous chapter, BT2 and BT4 show very close values, while the other specimens exhibit larger values. Whether this discrepancy is due to the variability in the material properties of bamboo culms or other causes remains a topic for future investigation.

Table 5: Tensile strain at either E or W point at maximum load in each bending test.

Species	Madake			Moso		
	BT1	BT2	BT3	BT4	BT5	BT6
	1.08%	0.73%	0.81%	0.69%	1.35%	1.20%
Mean	0.88%			1.08%		

5. Conclusion

A formulation based on the Brazier effect theory (BET) was conducted for the elastic stresses and strains in the fiber perpendicular direction that occur when bamboo culms undergo bending along the culm axis. The results of bending tests using specimens of Madake and Moso bamboo, compared with the BET values, showed good agreement, especially at locations not directly subjected to external forces. However, the strains in the fiber perpendicular direction at maximum load were often slightly higher than the maximum strains determined in preliminary experiments. Investigating the statistical values of these characteristics and their causes will be a subject for future research. Additionally, we aim to further develop a systematic approach to effectively utilize bamboo as a structural material for spatial structures.

Acknowledgements

Parts of the results of this study were supported by the Maeda Engineering Foundation Research Grant in fiscal years 2022 and 2023, and by a Grant-in-Aid for Scientific Research (21H0037: New Academic Fields Research, Plant-Structure-Optimization). Additionally, substantial assistance was received from students of The University of Shiga Prefecture, including Keisuke Oki, Yohei Nagano, Yu Kihara, and Ginto Tsukiyama. We express our heartfelt gratitude here.

References

[1] G. Minke, *Building with Bamboo: Design and Technology of a Sustainable Architecture*, 3rd ed., Birkhauser Architecture, Nov. 2022.

[2] N. V. Trong, *Towards a Reliable Bamboo Architecture - The Construction, Structure, and Space of Bamboo Architecture through the Use of Bundled Joints, Repeating Frame Units, and Bending Elements*, Doctoral Thesis, Graduate School of Creative Science and Engineering, Waseda University, Feb. 2022.

[3] "Plugin Connections and Bolt Structures," Available: https://bambus.rwth-aachen.de/eng/reports/connect/bolt/bolt.html (accessed on 31. Mar. 2024.)

[4] "Construction with Bamboo - Bamboo Connections," Available: https://bambus.rwth-aachen.de/eng/PDF-Files/Bamboo%20Connections.pdf (accessed on 31. Mar. 2024.)

[5] H. Toki and T. Nagai, "Design and construction of spatial structure using bamboo as structural materials –design and construction of emergency temporary building made of bamboo material (part 1)–," *AIJ Journal of Technology and Design*, vol. 21, no. 49, pp. 1007-1012, Oct. 2015, in Japanese. DOI: https://doi.org/10.3130/aijt.21.1007

[6] T. Nagai, K. Oki, Y. Nagano, and Y. Kihara, "Fundamental investigation on bending failure mechanism and bending strength of full-culm bamboo - comparative verification of bending stress generated in bamboo culm wall with Brazier effect theory, numerical analysis and experimental results," *Journal of Structural Engineering B*, vol. 69B, pp. 119-128, Apr. 2023, in Japanese. DOI: https://doi.org/10.3130/aijjse.69B.0_119

[7] H. Shima, M. Sato, and A. Inoue, "Self-adaptive formation of uneven node spacings in wild bamboo," *Physical Review E*, vol. 93, no. 2, Feb. 2016, https://doi.org/10.1103/PhysRevE.93.022406

[8] L.G. Brazier, "On the flexure of thin cylindrical shells and other thin sections," *Proceedings of the Royal Society of London*, A116, pp. 104-114, 1927.

[9] C. Calladine, *Theory of Shell Structures*, Cambridge University Press, 1983.

[10] T. Nagai, "Preliminary study on relationship between culm morphology and mechanical characteristics of Japanese bamboo," *Proceedings of the IASS Annual Symposium 2023 Integration of Design and Fabrication*, Melbourne, Australia, pp. 277-287, July 2023.

[11] ISO 22157, "Bamboo structures - Determination of physical and mechanical properties of bamboo culms -," 2019.

[12] S. Amada, T. Muneoka, Y. Nagase, Y. Ichikawa, A. Kirigai. and Y. Zhifei, "The mechanical structures of bamboos in viewpoint of functionally gradient and composite materials," *Journal of Composite Materials*, vol. 30, no. 7, pp. 800-819, 1996.

[13] K. Oki and T. Nagai, "Study on compression strength of Japanese full-culm bamboo columns using short-length specimens," *Proceedings of the IASS Annual Symposium 2023 Integration of Design and Fabrication*, Melbourne, Australia, pp. 288-296, July 2023.

[14] I. Ario, C. Morita, H. Suyama, E. Sato, and K. Fujii, "Mechanical considerations of the laminated composite structure modeled on the anisotropic organization of bamboo," *Transactions of the Japan Society of Mechanical Engineers Series A*, vol. 69, no. 677, pp. 148-153, 2003, in Japanese. DOI: https://doi.org/10.1299/kikaia.69.148

[15] J. Janssen, *Bamboo in Building Structures*, Doctoral Thesis, Eindhoven University of Technology, Netherlands, 1981.

[16] Y. Akinbade, *Mechanical and Morphological Characterization of Full-Culm Bamboo*, Doctoral thesis, Swanson School of Engineering, University of Pittsburgh, Mar. 2020.

[17] B. Sharma, K. A. Harries, and K. Ghavami, "Methods of determining transverse mechanical properties of full-culm bamboo," *Construction and Building Materials*, vol. 38, pp. 627-637, Jan. 2013.

[18] H. Horie, "Strength characteristics of bamboo culm ii. Estimation of strength properties of bamboo culm," *Mokuzai Gakkaishi*, vol. 67, no. 3, pp. 149-162, 2021, in Japanese. DOI: https://doi.org/10.2488/jwrs.67.149